

THE ROLE OF MOIST SHELLS IN DETERMINING THE DILUTION OF CUMULUS CLOUDS DUE TO TURBULENT MIXING

GUNHO (LOREN) OH* AND PHILIP H. AUSTIN
DEPARTMENT OF EARTH, OCEAN, AND ATMOSPHERIC SCIENCES
UNIVERSITY OF BRITISH COLUMBIA

1 Introduction

Clouds are surrounded by a moist shell that mediates mixing between their core and the environment. Observations of these shells have been made by , for example, Jonas (1990) and Rodts et al. (2003), who analyzed a large number of aircraft cloud transacts and observed the noted the existence of subsiding moist air surrounding the clouds, which is driven by mechanical forcing and evaporative cooling.

While these works focused primarily on the source of entrained air, recent modelling studies suggest that moist shells surrounding the cloud plays an important role in turbulent mixing processes. Dawe and Austin (2011b) suggests that traditional assumptions about mixing between the cloud and the environment are complicated by the existence of moist shells, which modifies the properties of the entrained and detrained air. The importance of moist shells surrounding the clouds is further highlighted by Yeo and Romps (2013), where the histories of Lagrangian particles are tracked and observed in a large-eddy simulation. They found that 61% of the entrainment events experienced by the Lagrangian particles are re-entrainment, where the moist shell acts as a conditioning stage, mediating the turbulent mixing between the cloud and the environment.

This means that the moist shell plays an important role in the way that clouds mix with the environment and become *diluted*. We define dilution rate due to entrainment and detrainment as a proportional change of a conserved tracer

ϕ , following Hannah (2017). Examining a series of single-bubble experiments, Hannah (2017) observed that the dilution rate was not a simple function of the directly calculated entrainment and detrainment rates. That is, the entrainment and detrainment rates do not represent the dilution of rising parcels.

We examine the role of moist shells in determining the rate of dilution for shallow and deep clouds modelled using a series of high-resolution, large-eddy simulations. Motivated by the works of Dawe and Austin (2011b) and Hannah (2017), we aim to resolve the discrepancies between directly calculated entrainment and detrainment rates (Dawe and Austin, 2011a; Romps, 2010) and bulk-plume estimates (Siebesma and Cuijpers, 1995) by investigating the role of moist shells in determining the properties of the entrained and detrained air, especially during more realistic simulations of shallow and deep cloud fields (Dawe and Austin, 2011b; Moser and Lasher-Trapp, 2017). Furthermore, the implications of the moist shells in convective parameterization will also need to be examined.

2 Methods

2.1 Model Description

The cloud statistics used here are from a series of high-resolution, large-eddy simulations (LES) using the System for Atmospheric Modelling (SAM; Khairoutdinov and Randall, 2003). We focus on two cases for the sake of the analysis,

loh@eoas.ubc.ca.

representing shallow and deep convection. The boundary-layer shallow cumulus case is based on the Barbados Oceanographic and Meteorology Experiment (BOMEX) case. The BOMEX LES model run has been performed with a grid spacing of 25 m, a time step of 1 second, over a $13 \text{ km} \times 13 \text{ km} \times 3.2 \text{ km}$ domain. The tropical marine deep convection case is based on GATE (Global Atmospheric Research Program (GARP) Atlantic Tropical Experiment Phase III; Houze Jr. and Betts, 1981); it has a domain size of $86.4 \text{ km} \times 86.4 \text{ km} \times 25.6 \text{ km}$, with 50 m model grid size in all directions and 2-second time step. The simulation was performed for 12 hours, and the last three hours are kept for analysis. Both model runs make use of a two-moment microphysics scheme developed by Morrison et al. (2005a,b).

We have implemented the direct entrainment calculation scheme of Dawe and Austin (2011a) to explicitly measure the rate of entrainment and detrainment. A version of the direct entrainment calculation developed by Kuang and Romps (2010) was also implemented, and we found that both methods yield equivalent rates for both entrainment and detrainment.

The results from LES runs then go through an extensive set of post-processing operations. The dataset is translated into a time series of three-dimensional fields, which are subsequently divided into three regions. We first define the cells with condensed liquid water ($q_n > 0$) as the *cloud* region, and further isolate the *cloud core* region, which are parts of the cloud region where the air is upward-moving ($w > 0$) and positively-buoyant ($B > 0$) (Dawe and Austin, 2011a). The shell is defined as the cloudy region surrounding the core, regardless of its dynamic properties. Interestingly, the properties of the shell with respect to the corresponding core is rather insensitive to the exact definition of the shell. Repeating the following analysis for moist downdrafts surrounding the shell, for example, yields the same result.

Individual clouds are then tracked using a modified cloud-tracking algorithm based on Dawe and

Austin (2012). This allows us to analyze the properties of the individual cloud core with respect to the corresponding shell. It is crucial, as we will describe later, to be able to observe the role of moist shells during cumulus convection.

2.2 Shell Correction

It has been well documented that directly calculated entrainment and detrainment rates are roughly twice the size of those calculated using conserved tracers (Dawe and Austin, 2011a,b; Kuang and Romps, 2010). It has been speculated that this discrepancy arises from the assumption made in Siebesma and Cuijpers (1995) that the air being entrained (detrained) has the properties of the mean environment (cloud core), respectively. That is, turbulent mixing during moist convection occurs directly between the cloudy air and the dry environment surrounding the cloud. Given the source of discrepancy between the directly calculated entrainment and detrainment rates (E_d, D_d) and the bulk-plume estimates (\bar{E}, \bar{D}), we implemented the shell correction method introduced by Dawe and Austin (2011b) to reproduce bulk-plume estimates for entrainment and detrainment rates using directly calculated quantities. To avoid confusion between the bulk-plume estimates based on Siebesma and Cuijpers (1995); Zhang et al. (2015) and the re-produced values using the shell correction method, we write the latter as (\tilde{E}, \tilde{D}) .

According to Dawe and Austin (2011b), the shell-corrected entrainment and detrainment rates, corresponding to the bulk-plumes estimates, can be calculated as:

$$(1a) \quad \tilde{E} = E_d - \left(E_d \frac{\phi_e - \bar{\phi}}{\phi_c - \bar{\phi}} + D_d \frac{\phi_c - \phi_d}{\phi_c - \bar{\phi}} \right)$$

$$(1b) \quad \tilde{D} = D_d - \left(E_d \frac{\phi_e - \bar{\phi}}{\phi_c - \bar{\phi}} + D_d \frac{\phi_c - \phi_d}{\phi_c - \bar{\phi}} \right)$$

where ϕ_c and $\bar{\phi}$ are the thermodynamic properties of the cloud core and the mean environment, respectively, and ϕ_e and ϕ_d are flux-averaged quantities of the entrainment and detrained air $\phi_e = (E\phi)_d/E_d$ and $\phi_d = (D\phi)_d/D_d$.

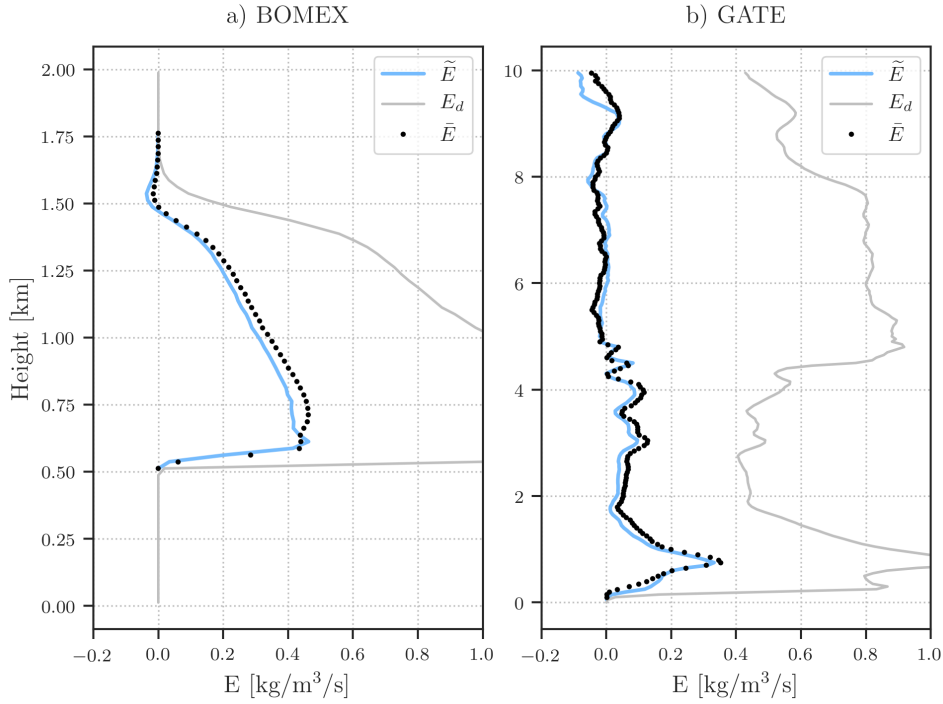


FIGURE 1. Comparison between the direct entrainment rates (grey) and the shell-corrected values (light blue), as well as the bulk-plume estimates (dotted line). The bulk-plume estimates are calculated according to Siebesma and Cuijpers (1995) for BOMEX (left), and Zhang et al. (2015) for GATE case (right).

2.3 Dilution Calculation

The goal of this study is to precisely determine how the assumptions made in calculating the entrainment and detrainment estimates relate to the idea of dilution. While most convective parameterization schemes make the assumption that entrainment is synonymous with dilution, the exact relationship between the two remains ambiguous (Dawe and Austin, 2011b; Hannah, 2017).

How does one describe the dilution due to entrainment and detrainment using the direct calculation methods, without averaging out the effect of moist shell during turbulent mixing? Hannah (2017) quantifies the rate of dilution due to entrainment and detrainment using directly diagnosed values. That is, by rearranging the mass-continuity equations (*cf.* Roms, 2010), the total dilution of a generic, (quasi-)conserved tracer ϕ

for the individual cloud volumes can be written as

$$(2) \quad \frac{1}{\phi'_c} \frac{\partial \phi_c}{\partial t} + \frac{w_c}{\phi'_c} \frac{\partial \phi_c}{\partial z} = - \frac{\langle e \rangle (\phi_c - \phi_e)}{\langle \rho \phi' \mathcal{A} \rangle} + \frac{\langle d \rangle (\phi_c - \phi_d)}{\langle \rho \phi' \mathcal{A} \rangle} + \langle \mathcal{A} S_\phi \rangle$$

where \mathcal{A} is an activity operator that is one for cloudy region and zero otherwise, ϕ_c is the tracer averaged over the cloud region, ϕ_e and ϕ_d are flux-averaged values of the tracer for entrained and detrained air, and S_ϕ denotes all sources and sinks of the tracer ϕ . For a more detailed explanation and derivation of Equation (2), refer to Hannah (2017); Roms (2010).

The expression (Equation (2)) represents the proportional changes in a conserved tracer ϕ for each cloud volume due to entrainment (first term on the right-hand side) and detrainment (second term) as well as large-scale forcing (third term). The dilution rates are given in units of [s^{-1}], and can be thought of as a timescale during which a

volume of moist air dilutes and becomes as dry as the surrounding environment.

The source/sink term $\langle AS_\phi \rangle$ is not negligible (cf. Hannah (2017)), but since we are only interested in the effect of entrainment and detrainment, especially during the turbulent mixing processes, we decided to ignore the effect of large-scale forcing term for the time being.

3 Results

3.1 Bulk vs Direct Entrainment

Figure 1 gives the results of applying the shell correction method on BOMEX (left panel) and GATE (right panel) cases. The transformed bulk-plume estimates (\tilde{E}, \tilde{D}) show a good agreement with (\bar{E}, \bar{D}) . As such, we will be using (\tilde{E}, \tilde{D}) values for individual clouds to estimate the bulk-plume entrainment and detrainment rates. The method provides a way to transform the unbiased, directly-calculated entrainment and detrainment rates into the bulk-plume estimates with the assumptions used for basic entraining-plume parameterization schemes.

The shell correction method is useful as the calculations can be performed for the individually-tracked clouds. This allows us to directly compare the directly calculated entrainment and detrainment rates to bulk-plume estimates as well as the rate of cloud core dilution.

3.2 Dilution due to Entrainment

We have performed the calculation of dilution rates for the individual clouds observed during BOMEX and GATE. The vertical distribution of dilution rates due to entrainment (first term on the right-hand side of Equation (2)) is shown in Figure 2. The result of calculating the dilution rates according to Equation (2) is consistent for both BOMEX and GATE cases, as well as that of Hannah (2017).

Taking the inverse of the calculated rate of dilution gives the dilution timescale τ_Ω , which represents the time a parcel takes to dilute and become

as dry as the large-scale environment. The variability in τ_Ω is quite large, but on average, the dilution timescale is roughly 5-20 minutes for shallow clouds, and 10-45 minutes for deep clouds.

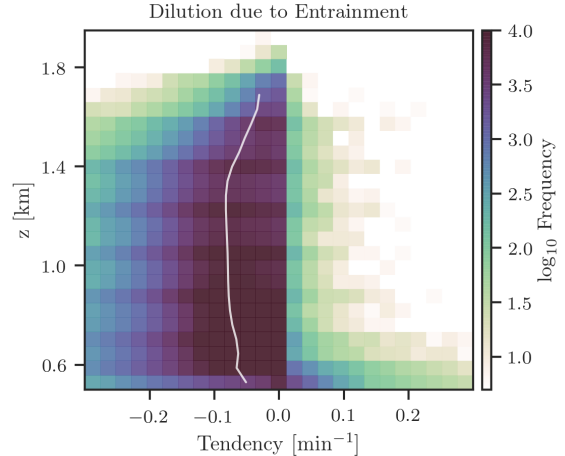


FIGURE 2. Vertical distribution of entrainment tendency (first term on the right-hand side of Equation (2)). Each data point in the two-dimensional histogram corresponds to the rate of dilution due to entrainment at each height for the individual clouds. The white curve denotes the mean distribution, and the colours represent the number of cloud samples.

The dilution timescales τ_Ω are a bit longer than the values reported by Hannah (2017), but still close to the observed lifetimes of cumulus clouds. We assume this is because of the nature of single-plume experiments, where the air being entrained into the target plume is drier than that of the cloud field.

3.3 Bulk Entrainment vs Dilution

In order to investigate the exact relationship between the bulk-plume entrainment rate \bar{E} and the rate of dilution due to entrainment, we applied the bulk-plume approximation to the calculation of dilution rate (Equation (2)). That is, the directly-calculated entrainment and detrainment rates (E_d, D_d) were replaced with bulk-plume rates $(\bar{E}, \bar{D}) \simeq (\tilde{E}, \tilde{D})$ and the entrained (detrained) air

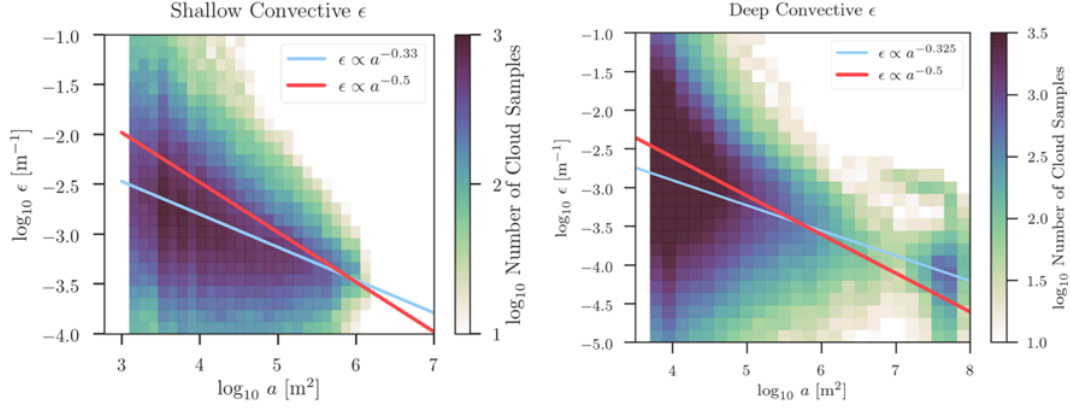


FIGURE 3. Comparison of the fractional entrainment $\epsilon = E/M$ rates versus cloud size for BOMEX (left) and GATE (right) cases. The colours represent \log_{10} cloud samples, where each individual sample corresponds to (a, ϵ) pair calculated for individually-tracked clouds at each height. The linear regression of the two-dimensional histogram is drawn in light blue, and a curve corresponding to $\epsilon \propto a^{0.5}$ in red.

is assumed to have the properties of the environmental (cloud core) air. Surprisingly, the resulting distribution appears almost exactly the same of Figure 2, but only slightly smaller in magnitude.

We can write the right-hand side of Equation (2) as

$$(3) \quad \Omega_e + \Omega_d = -\frac{\langle e \rangle (\phi_c - \phi_e)}{\langle \rho \phi' \mathcal{A} \rangle} + \frac{\langle d \rangle (\phi_c - \phi_d)}{\langle \rho \phi' \mathcal{A} \rangle}$$

where (Ω_e, Ω_d) denote the rates of dilution due to entrainment and detrainment, respectively.

Then we can apply the bulk-plume approximations, which gives

$$(4) \quad \begin{aligned} \Omega_d + \Omega_d &= -\frac{\langle \tilde{e} \rangle (\phi_c - \bar{\phi})}{\langle \rho \phi' \mathcal{A} \rangle} + \frac{\langle \tilde{d} \rangle (\phi_c - \phi_c)}{\langle \rho \phi' \mathcal{A} \rangle} \\ &= -\frac{\langle \tilde{e} \rangle (\phi_c - \bar{\phi})}{\langle \rho \phi' \mathcal{A} \rangle} \end{aligned}$$

but $\phi'_c = \phi_c - \bar{\phi}$ by definition. Since $\bar{\phi}$ is simply a domain-averaged value of ϕ and since $\phi_c = \langle \rho \phi \mathcal{A} \rangle / \langle \rho \mathcal{A} \rangle$, or the average of ϕ over the individual cloud area, the anomaly in ϕ_c is merely $\phi'_c = \langle \rho \phi' \mathcal{A} \rangle / \langle \rho \mathcal{A} \rangle$, which means

$$(5) \quad \begin{aligned} \Omega_e + \Omega_d &= -\frac{\langle \tilde{e} \rangle}{\langle \rho \mathcal{A} \rangle} \\ \Omega &= -\frac{1}{\rho} \tilde{E} \end{aligned}$$

where the right-hand side of the equation reduces to the *average* bulk-plume entrainment rate divided by the average density of the individual cloud core. We have further simplified the expression by writing the total dilution due to entrainment and detrainment as $\Omega = \Omega_e + \Omega_d$.

The extra density term is likely because we divided both sides of the dilution equation (Equation (2)) by $\langle \rho \phi' \mathcal{A} \rangle$, not by the total anomaly $\langle \phi' \mathcal{A} \rangle$. Nevertheless, it is clear that the rate of dilution due to entrainment and detrainment is not only equivalent, but identical to the bulk-plume entrainment estimate, as shown in Equation (5). It is also possible to rearrange the right-hand side of Equation (2) to derive the shell correction calculation for entrainment (Equation (1a)), which is not surprising, because ideally, the shell-corrected mass flux rates should be the bulk-plume estimates (i.e. $(\bar{E}, \bar{D}) \equiv (\tilde{E}, \tilde{D})$).

Examining the dilution equation under the bulk-plume assumptions explains the relationship between the directly-calculated entrainment and detrainment rates with the bulk-plume estimates. The bulk-plume entrainment and detrainment rates are arbitrarily adjusted to force the assumptions about the properties of the entrained and detrained air ($\phi_e = \bar{\phi}$ and $\phi_d = \phi_c$). Because

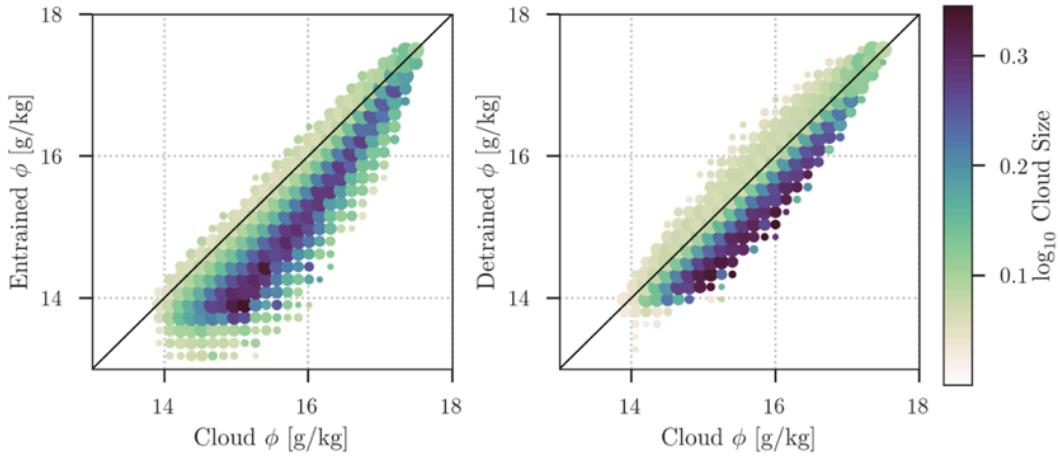


FIGURE 4. Comparison between the cloud core specific humidity $\phi_c = \bar{q}_t^c$, the entrained air (left), and the detrained air (right). The black line represents where the cloud core property is the same as the entrained (left) and the detrained (right) air. The colours show the horizontal size in $[\text{km}^2]$ of the cloud core in each bin.

these values are not realistic (see Section 3.5), the bulk-plume estimates of entrainment and detrainment rates are not physical properties of the turbulent mixing process, but intentionally tuned to produce the correct rate of dilution (*cf.* Equation (5)). Note that in this framework, detrainment does not contribute to the dilution of the cloud volume.

3.4 Size Dependence

Given that the bulk-plume estimate of the entrainment rate gives the right dilution rate, we are also interested in its implications on cumulus parameterization schemes. Most operational large-scale models take a rather crude approach, where the fractional entrainment rate ($\epsilon = E/M$) is inversely proportional to cloud size. This relationship is the centrepiece of the widely-used one-dimensional entraining plume model, developed by Simpson et al. (1965) and Simpson (1971); Simpson and Wiggert (1969) and has been tested against laboratory water tank experiments (See Turner, 1963).

The use of cloud size as a proxy for fractional entrainment rate (and sometimes for fractional detrainment rate δ as well; for example, see Tiedtke (1989)) is still popular today with

bulk-plume convective parameterization schemes (Bechtold et al., 2008; Bretherton et al., 2004; Jakob and Siebesma, 2003; Kain and Fritsch, 1990; Tiedtke, 1989). These traditional schemes use a fixed value (*i.e.* proxy) for the cloud ensemble, based on a radius of $R \simeq 500$ m for shallow convection, and $R \simeq 1500$ m for deep convection (Kain and Fritsch, 1990).

Calculating individual cloud entrainment rates under the bulk-plume assumption reveals that the inverse relationship is not very strong (Figure 3) both during shallow (left panel) and deep convection (right panel). While it is true that larger clouds entrain relatively less than smaller ones, the effect of horizontal scale on entrainment seems to be on the weak side. We could argue that the relationship still holds with a slightly adjusted parameter $\epsilon \propto a^{-0.3}$, but the variability in the distribution is too large, and the smallest clouds could yield both the smallest and the highest (fractional) entrainment rates. This observation applies directly to the size dependence of the rate of dilution as well (not shown).

3.5 Properties of Moist Shell

Why is entrainment (and equivalently, dilution) not a strong function of cloud size? It appears that

although the (fractional) rate of entrainment is probably the most important parameter in a convective parameterization scheme used in large-scale simulations (Siebesma and Cuijpers, 1995), validity of the inverse relationship seems insubstantial (Emanuel, 1994, p. 540). Perhaps it is not too surprising that even from the earliest observational studies, the robustness of the inverse relationship has been questioned (Sloss, 1967).

Given that the rate of dilution in a cloud volume due to entrainment is essentially a function of entrainment rate, the property of the cloud ϕ_c and of the entrained air ϕ_e , perhaps it is worth looking at the relative characteristics of the cloud properties with respect to cloud size.

In Figure 4, We have plotted the relative characteristics of the cloud core air and the entrained air (left panel) and of the cloud core air and the detrained air (right panel). Without looking at the cloud size distribution, it appears that the entrained air is almost always drier than the mean cloud core, while the properties of the detrained air are similar to the cloud core, which is similar to bulk-plume approximations. Interestingly, it is evident that larger clouds seemingly entrain and detrain the air that is exclusively drier than the cloud core. This is likely because the width of the moist shell is relatively smaller for larger clouds, allowing more dry environmental air to be mixed directly with the cloud.

This means that larger clouds experience concentration due to detrainment, slightly balancing out dilution due to entrainment, which might explain why larger clouds are not diluting as slowly as expected. For larger clouds, the entrained air is relatively drier than the detrained air (because the detrained air properties are much closer to the cloud core average quantities; *cf.* Figure 4). So the dilution rate decreases with cloud size, but more slowly than anticipated by the inverse relationship.

4 Discussion

We investigated the role of moist shells for individually observed clouds from BOMEX and GATE case simulations, especially in modulating the properties of the entrained and detrained air during turbulent mixing processes.

Using the shell correction method (Dawe and Austin, 2011b) to translate directly-calculated entrainment and detrainment rates (E_d, D_d) into equivalent bulk-plume estimates $(\bar{E}, \bar{D}) \simeq (\tilde{E}, \tilde{D})$, we have found that the rate of dilution for a cloud volume is identical to the bulk-plume entrainment estimate. This is, however, not to say that bulk-plume estimates used in convective parameterization schemes will produce the right amount of dilution. Previous studies already report that this is not the case (Dawe and Austin, 2013; Romps, 2010), and the parameterization schemes cannot reproduce the variability in the individual cloud properties within a cloud ensemble.

We further examined the effect of cloud size on both entrainment and dilution rates, but did not find a strong evidence for the widely-used inverse relationship. The results agree with previous observational studies where larger clouds dilute more slowly than smaller ones, but given a large variability in both entrainment and dilution rates, the robustness of the inverse relationship is rather questionable.

The existence of moist shells regulating the turbulent mixing processes between the clouds and the surrounding environment can explain this discrepancy. Because the relative properties of the entrained and detrained air depends on cloud size, the net effect of entrainment and detrainment on the rate of dilution of a cloud volume depends on the size of the cloud. Larger clouds seem to preferentially entrain dry air, because the relative size of the shell becomes smaller as clouds grow.

Given the exact rate of dilution as well as the correct lateral fluxes, it is possible to model a hypothetical mixing process where the bulk-plume

assumption is true. That is, we can adjust the dilution parameters so that entrainment always dilutes the cloud, and the effect of detrainment is ignored. Will this entrainment rate be inversely proportional to cloud size, unlike the bulk-plume entrainment estimate, where the effect of entrainment and detrainment is implicitly considered, but adjusted to match the lateral fluxes? It is, however, not the focus of this study. We hope to implement such a model and investigate the implications on the large-scale convective parameterization in a future study.

Acknowledgements

This research was made possible in part by the support provided by the Microsoft Azure for Research Program and Compute Canada.

References

- Bechtold, P., M. Köhler, T. Jung, F. Doblas Reyes, M. Leutbecher, M. J. Rodwell, F. Vitart, and G. Balsamo, 2008: Advances in simulating atmospheric variability with the ECMWF model: From synoptic to decadal time-scales. *Q. J. R. Meteorol. Soc.*, **134 (634)**, 1337–1351.
- Bretherton, C. S., J. R. McCaa, and H. Grenier, 2004: A New Parameterization for Shallow Cumulus Convection and Its Application to Marine Subtropical Cloud-Topped Boundary Layers. Part I: Description and 1D Results. *Mon. Wea. Rev.*, **132 (4)**, 864–882.
- Dawe, J. T. and P. H. Austin, 2011a: Interpolation of LES Cloud Surfaces for Use in Direct Calculations of Entrainment and Detrainment. *Mon. Wea. Rev.*, **139 (2)**, 444–456.
- Dawe, J. T. and P. H. Austin, 2011b: The Influence of the Cloud Shell on Tracer Budget Measurements of LES Cloud Entrainment. *J. Atmos. Sci.*, **68 (12)**, 2909–2920.
- Dawe, J. T. and P. H. Austin, 2012: Statistical analysis of an LES shallow cumulus cloud ensemble using a cloud tracking algorithm. *Atmos. Chem. Phys.*, **12 (2)**, 1101–1119.
- Dawe, J. T. and P. H. Austin, 2013: Direct entrainment and detrainment rate distributions of individual shallow cumulus clouds in an LES. *Atmos. Chem. Phys.*, **13 (15)**, 7795–7811.
- Emanuel, K. A., 1994: *Atmospheric Convection*. Oxford University Press.
- Hannah, W. M., 2017: Entrainment versus Dilution in Tropical Deep Convection. *J. Atmos. Sci.*, **74 (11)**, 3725–3747.
- Houze Jr., R. A. and A. K. Betts, 1981: Convection in GATE. *Rev. Geophys.*, **19 (4)**, 541–576.
- Jakob, C. and A. P. Siebesma, 2003: A New Subcloud Model for Mass-Flux Convection Schemes: Influence on Triggering, Updraft Properties, and Model Climate. *Mon. Wea. Rev.*, **131 (11)**, 2765–2778.
- Jonas, P. R., 1990: Observations of cumulus cloud entrainment. *Atmos. Res.*, **25 (1-3)**, 105–127.
- Kain, J. S. and J. M. Fritsch, 1990: A One-Dimensional Entraining/Detraining Plume Model and Its Application in Convective Parameterization. *J. Atmos. Sci.*, **47 (23)**, 2784–2802.
- Khairoutdinov, M. F. and D. A. Randall, 2003: Cloud Resolving Modeling of the ARM Summer 1997 IOP: Model Formulation, Results, Uncertainties, and Sensitivities. *J. Atmos. Sci.*, **60 (4)**, 607–625.
- Kuang, Z. and D. M. Romps, 2010: Nature versus Nurture in Shallow Convection. *J. Atmos. Sci.*, **67 (5)**, 1655–1666.
- Morrison, H., J. A. Curry, and V. I. Khvorostyanov, 2005a: A New Double-Moment Microphysics Parameterization for Application in Cloud and Climate Models. Part I: Description. *J. Atmos. Sci.*, **62 (6)**, 1665–1677.
- Morrison, H., J. A. Curry, M. D. Shupe, and P. Zuidema, 2005b: A New Double-Moment Microphysics Parameterization for Application in Cloud and Climate Models. Part II: Single-Column Modeling of Arctic Clouds. *J. Atmos. Sci.*, **62 (6)**, 1678–1693.
- Moser, D. H. and S. Lasher-Trapp, 2017: The Influence of Successive Thermals on Entrainment

- and Dilution in a Simulated Cumulus Congestus. *J. Atmos. Sci.*, **74 (2)**, 375–392.
- Rodts, S. M. A., P. G. Duynkerke, and H. J. J. Jonker, 2003: Size Distributions and Dynamical Properties of Shallow Cumulus Clouds from Aircraft Observations and Satellite Data. *J. Atmos. Sci.*, **60 (16)**, 1895–1912.
- Romps, D. M., 2010: A Direct Measure of Entrainment. *J. Atmos. Sci.*, **67 (6)**, 1908–1927.
- Siebesma, A. P. and J. W. M. Cuijpers, 1995: Evaluation of Parametric Assumptions for Shallow Cumulus Convection. *J. Atmos. Sci.*, **52 (6)**, 650–666.
- Simpson, J., 1971: On Cumulus Entrainment and One-Dimensional Models. *J. Atmos. Sci.*, **28 (3)**, 449–455.
- Simpson, J., R. H. Simpson, D. A. Andrews, and M. A. Eaton, 1965: Experimental cumulus dynamics. *Rev. Geophys.*, **3 (3)**, 387.
- Simpson, J. and V. Wiggert, 1969: Models of Precipitating Cumulus Towers. *Mon. Wea. Rev.*, **97 (7)**, 471–489.
- Sloss, P. W., 1967: An Empirical Examination of Cumulus Entrainment. *J. Appl. Meteor.*, **6 (5)**, 878–881.
- Tiedtke, M., 1989: A Comprehensive Mass Flux Scheme for Cumulus Parameterization in Large-Scale Models. *Mon. Wea. Rev.*, **117 (8)**, 1779–1800.
- Turner, J. S., 1963: The motion of buoyant elements in turbulent surroundings. *J. Fluid. Mech.*, **16 (01)**, 1.
- Yeo, K. and D. M. Romps, 2013: Measurement of Convective Entrainment Using Lagrangian Particles. *J. Atmos. Sci.*, **70 (1)**, 266–277.
- Zhang, G. J., X. Wu, X. Zeng, and T. Mitovski, 2015: Estimation of convective entrainment properties from a cloud-resolving model simulation during TWP-ICE. *Clim. Dyn.*, **47 (7-8)**, 2177–2192.